

UCLA

UCLA Previously Published Works

Title

Noise Analysis of Closed-Loop Vibratory Rate Gyros

Permalink

<https://escholarship.org/uc/item/9qd51961>

ISBN

978-1-4577-1095-7

Authors

Kim, Dennis
M'Closkey, Robert

Publication Date

2012

Peer reviewed

Noise Analysis of Closed-Loop Vibratory Rate Gyros

Dennis Kim* and Robert M'Closkey†
Mechanical and Aerospace Engineering Department
University of California, Los Angeles

Abstract—This paper presents detailed noise analysis of closed-loop MEMS vibratory gyros whose noise characteristics are dominated by the mechanical-thermal noise of the sensor's vibrating structure as well as the electrical noise associated with the pickoff signal conditioning electronics in the sense channel. The mechanical-thermal noise and the electrical noise are represented as uncorrelated additive wideband disturbances dominant at the sensor's input and output, respectively. A comprehensive spectral density model of the closed-loop rate-equivalent noise is derived to explain the effects of various sensor parameters including the resonator quality factor, the closed-loop bandwidth, and the modal frequency split. Experimental results with a Disk Resonator Gyro (DRG) are presented to support the analysis.

I. INTRODUCTION

Vibratory rate gyros detect angular rate of rotation by exploiting two lightly damped Coriolis-coupled modes in the sensor's vibrating structure. Tuned, open-loop, vibratory gyros yield the optimum noise performance, however, the sensor's bandwidth is limited in devices with high Q resonators. Thus, closed-loop operation is an effective way to extend the sensor bandwidth, and our book chapter [4] provides extensive and detailed derivation of open- and closed-loop gyro noise spectra with respect to electrical noise introduced by the pickoff signal conditioning electronics. The present paper extends the analysis of [4] to include both signal conditioning noise and mechanical-thermal noise of the resonator. The results are interesting for two reasons. First, mechanical-thermal noise can often be measured in vibratory gyros, especially those categorized as "MEMS" devices, so this noise source should be included in any analysis. Second, from the perspective of modeling, mechanical-thermal noise enters into the system in a different location than the signal conditioning or "electronic" noise and, thus, cannot be accounted for by simply perturbing the intensity of the electronic noise. Analysis of the angular rate noise was performed in [6] considering only mechanical-thermal noise, however, a complete analysis must necessarily include both noise sources. Indeed, both noise sources are quite evident in the open-loop noise spectra associated with Boeing's Disk Resonator Gyro (DRG) discussed in Sec. III.

The paper is organized as follows. Section II presents a detailed spectral density model of the closed-loop rate-equivalent noise and discusses effects that various sensor

parameters such as modal quality factor, bandwidth, and modal frequency detuning, have on the rate-equivalent noise as well as the angle random walk. Experimental results with the Boeing DRG are provided in Section III and Section IV concludes the paper.

II. NOISE ANALYSIS

The fundamental model of a vibratory gyro is two degree-of-freedom resonator with a Coriolis coupling term modulated by the sensor's angular velocity. When the equations of motion are written in the sensor fixed coordinates, denoted $x = [x_1, x_2]^T$ where x_1 and x_2 represent the generalized coordinates of the resonator, the linear mechanics can be described by the following two degree-of-freedom model,

$$M\ddot{x} + C\dot{x} + \alpha\Omega S\dot{x} + Kx = f \quad (1)$$

where $f = [f_{exc}, f_{reb}]^T$ are generalized forces, M , C , and K are real, positive definite 2-by-2 mass, damping, and stiffness matrices, respectively. S is a skew-symmetric matrix

$$S = \begin{bmatrix} 0 & -1 \\ 1 & 0 \end{bmatrix}$$

that couples the angular rate of rotation, Ω , between the two vibratory modes with the coupling strength α . In closed-loop operation, a feedback loop, called an excitation loop, establishes a stable oscillation of the x_1 degree-of-freedom and a second feedback loop, called the force-to-rebalance loop, nulls the x_2 degree-of-freedom and rejects the disturbance injected by the Coriolis coupling. The angular rate of rotation is then estimated by demodulating the rebalance feedback signal with respect to a phase-shifted copy of the excitation signal. Measurement of x_1 is called the "drive" signal, and measurement of x_2 is called the "sense" signal. Noise in the demodulated signals, whether running the sensor open- or closed-loop, limits the accuracy of the estimated angular rotation rate. For the noise analysis in this paper, the following assumptions are made,

- 1) The open-loop dynamics of the sensor can be viewed as a 2-input/2-output system, i.e. from f to x . Cross-channel coupling between the excitation and sense channels is ignored since the cross-channel peak gain is typically a few orders of magnitude smaller than the diagonal term when the sensor is effectively decoupled. Furthermore, cross-channel coupling is more related to longer-term trends in the zero-rate rate bias that is not correlated with the noise. Thus, the x/f transfer

* Email: dongj@seas.ucla.edu

† Corresponding author. Email: rtm@seas.ucla.edu. This work is supported by DARPA contract W31P4Q-10-1-0017.

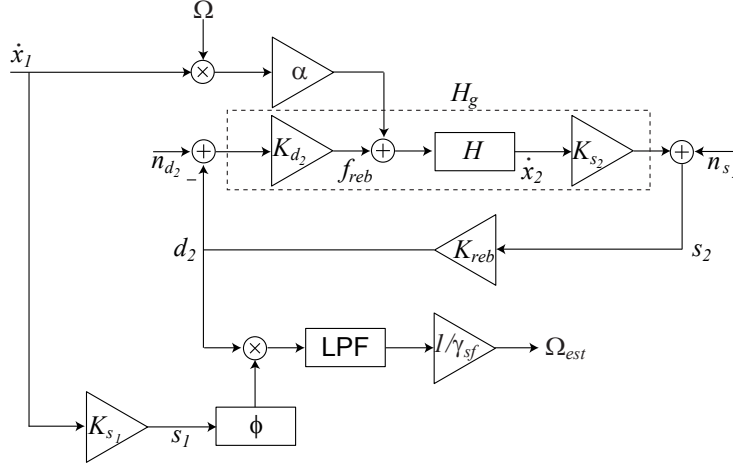


Fig. 1. Block diagram of closed-loop sense channel. Also shown is the demodulation which produces the estimated rate, denoted Ω_{est} . The excitation control loop (not shown here) establishes $x_1(t) = a \cos(\omega_0 t)$ [m]. The force-to-rebalance loop nulls the measurement of the x_2 degree-of-freedom whether produced by an angular rate “disturbance” (labeled Ω) or the noise sources (labeled as n_{d_2} and n_{s_2}). The fundamental sensor mechanics of the rebalance channel is denoted H and the input and output signal conditioning dynamics are represented as simple conversion constants, K_{d_2} and K_{s_2} , respectively. The rebalance control element is also represented as a simple constant K_{reb} for the noise analysis. The input noise, n_{d_2} , whose intensity is v [V/rt-Hz] represents the voltage-equivalent mechanical-thermal noise, and the output noise, n_{s_2} , whose intensity is μ [V/rt-Hz] represents the electrical noise associated with the pickoff electronics. The estimated angular rate, denoted Ω_{est} , is determined by demodulating d_2 with respect to a phase-shifted copy of s_1 . K_{s_1} is the conversion constant associated with the output signal conditioning dynamics in the excitation channel and ϕ , “LPF”, and γ_{sf} denote the phase shift, Low Pass Filter, and scale factor, respectively.

function is assumed to be essentially diagonal. The x_1/f_{exc} diagonal term is called the *drive channel* and x_2/f_{reb} transfer function is called the *sense channel*. The drive and sense channel transfer function magnitudes are much larger than the x_1/f_{reb} and x_2/f_{exc} transfer function magnitudes under our assumption.

- 2) The excitation feedback loop perfectly regulates the x_1 degree-of-freedom to a constant amplitude sinusoidal response $x_1(t) = a \cos(\omega_0 t)$, where a is the amplitude and ω_0 is the excitation frequency. The excitation frequency, which is primarily dictated by the drive channel transfer function, may be different from the modal frequency associated with the sense channel, i.e. the dominant mode in x_2/f_{reb} . Due to the relatively large amplitude and stability of x_1 , the noise contribution of this excitation signal to the demodulated signal is ignored and only the noise associated with the sense channel signal is considered in the analysis.
- 3) Signal conditioning noise is represented as an additive wideband disturbance at the sense channel output. For sensors like the DRG, in which a transresistance amplifier is used to provide the buffering of the electrode charge into a low impedance voltage, the electrical noise is dominated by the Johnson noise [3] of the feedback resistor across the op amp. The square root spectral density of this source is given by

$$\sqrt{4k_B T R} \quad [\text{V/rt-Hz}]$$

where k_B is Boltzmann’s constant, T is the absolute temperature in Kelvin, and R is resistor’s value in ohms. We use μ , expressed in V/rt-Hz, to represent this constant spectral density.

- 4) The spectral density of mechanical-thermal noise [2] is given by

$$\sqrt{4k_B T c} \quad [\text{N/rt-Hz}]$$

where c is the mechanical-resistance or damping associated with the sense channel mode, expressed in N/m/s. This noise source can be viewed as a disturbance force located at the input to the resonator. Due to the difficulty in predicting the damping in MEM resonators, though, an empirical approach is adopted in which the mechanical-thermal noise is represented as a wideband, flat spectrum, disturbance voltage located at the input of the measured sense channel’s transfer function. The spectral density is denoted v and is expressed in V/rt-Hz. In practice, v is calculated by selecting its value so that $|H_g|v$ matches the measured open-loop noise spectrum of the sense channel in a neighborhood of the sense channel modal frequency (see Fig. 1 for notation).

- 5) Our final assumption is that the input signal conditioning dynamics can be treated as simple noiseless conversion constant. The output signal conditioning dynamics contribute the Johnson noise mentioned above.

Fig. 1 shows the block diagram corresponding to the closed-loop sense channel with the aforementioned assumptions. If m , c , and k are the modal mass, damping, and stiffness parameters associated with H in Fig. 1, then the sense channel transfer function including the input and output dynamics (the gains K_{s_2} and K_{d_2}), denoted H_g , is given by

$$H_g(s) = \frac{K_{s_2} K_{d_2}}{m} \frac{s}{s^2 + 2\sigma s + \omega_n^2} \quad (2)$$

where $\omega_n = \sqrt{k/m}$ is the undamped natural frequency and $\sigma = c/(2m) = \omega_n/(2Q)$ is the resonator's mechanical bandwidth with the modal quality factor Q . The peak gain of (2) at $\omega = \omega_n$ is defined as

$$h = |H_g(j\omega_n)| = \frac{K_{s_2}K_{d_2}}{2\sigma m}.$$

Before analyzing the rate-equivalent noise of the estimated rate signal, it is useful to consider the noise associated with the rebalance loop feedback signal, d_2 . The overall noise density of d_2 prior to demodulation, denoted S_{d_2} , is computed to be

$$S_{d_2}(\omega) = \left| \frac{K_{reb}}{1 + K_{reb}H_g(j\omega)} \right| \times \sqrt{\mu^2 + |H_g(j\omega)|^2 v^2} \quad [\text{V/rt-Hz}]. \quad (3)$$

This spectrum displays a deep notch, whose minimum is located at ω_n , when the resonator quality factor is high.

The rate-equivalent noise is determined by demodulating the noise spectrum of d_2 with the phase-shifted copy of s_1 and then normalizing by the scale factor. Note that in this treatment, where the dynamics of input and output buffers have been ignored, the ideal demodulation phase ϕ is zero. As an intermediate step we scale the spectral density (3) by the s_1 amplitude and normalize by the scale factor to produce

$$\begin{aligned} \frac{K_{s_1}a\omega_0}{\gamma_{sf}(\omega_0)} S_{d_2}(\omega) &= \frac{4\sigma m}{K_{s_2}\alpha a\omega_0} \\ &\times \sqrt{\frac{\left(\frac{\omega_n^2 - \omega_0^2}{2\omega_0}\right)^2 + \sigma_{clp}^2}{\sigma^2}} \\ &\times \sqrt{\frac{\left(\frac{\omega_n^2 - \omega^2}{2\omega}\right)^2 \mu^2 + \sigma^2 (\mu^2 + h^2 v^2)}{\left(\frac{\omega_n^2 - \omega^2}{2\omega}\right)^2 + \sigma_{clp}^2}} \end{aligned} \quad (4)$$

where the unit of this spectral density is deg/hr/rt-Hz. The closed-loop scale factor, denoted γ_{sf} , is derived to be (see [4])

$$1/\gamma_{sf}(\omega_0) = \frac{4m}{\alpha K_{s_1} a^2 \omega_0^2 K_{s_2} K_{reb}} \sqrt{\left(\frac{\omega_n^2 - \omega_0^2}{2\omega_0}\right)^2 + \sigma_{clp}^2}$$

where σ_{clp} is the closed-loop bandwidth,

$$\sigma_{clp} = \sigma + K_{reb} \frac{K_{s_2} K_{d_2}}{2m}.$$

The closed-loop bandwidth is adjusted by the rebalance loop controller gain K_{reb} . Expression (4) is useful because it expresses the spectral density of the sense channel noise with units of angular rotation rate. Furthermore, the scale factor is well approximated by

$$1/\gamma_{sf}(\omega_0) \approx \frac{2K_{d_2}}{K_{s_1}\alpha a^2 \omega_0^2}$$

assuming $\sigma_{clp} \gg \sigma$, i.e. the closed-loop bandwidth is larger than the open-loop bandwidth, and $\sigma_{clp} > |\omega_0 - \omega_n|$, i.e. the closed-loop bandwidth is larger than the detuning

frequency $\Delta := |\omega_0 - \omega_n|$. Both of these assumptions are quite reasonable in practice because the whole point of using feedback around the sense channel is to achieve a larger bandwidth than that provided by the open-loop sensor dynamics, and the detuning frequency is typically small relative to the σ_{clp} because in "tuned" sensors the objective is to make $\Delta \approx 0$. With regard to the latter condition, high performance vibratory gyros typically require $\Delta < 1$ Hz, which is at least an order of magnitude smaller than σ_{clp} . Under these two conditions (4) is essentially independent of ω_0 and its minimum value is achieved at frequency $\omega = \omega_n$ and is given by

$$\frac{4\sigma m}{K_{s_2}\alpha a\omega_n} \sqrt{\mu^2 + h^2 v^2}. \quad (5)$$

In other words, (5) is the value of (4), expressed in deg/hr/rt-Hz, at deepest part of the notch (see Fig. 6(a)).

The noise spectrum of the estimated angular rate is obtained by demodulating (4) with a unit amplitude sinusoid at ω_0 . The low-pass filter, shown as the "LPPF" block in Fig. 1, limits the bandwidth of the demodulated signal. The equivalent effect of the low-pass filter on the spectral density (4) is to filter this spectrum with a bandpass filter possessing twice the low-pass filter bandwidth and with center frequency at ω_0 . Because ω_0 is typically at least an order of magnitude larger than the low-pass filter bandwidth, the filtered spectrum can be treated as a narrowband or quasimonochromatic process. The demodulated signal's spectrum is then a simple function of the narrowband spectrum (see [7]),

$$S_{\Omega}(\omega) = \frac{K_{s_1} a \omega_0}{\sqrt{2} \gamma_{sf}(\omega_0)} \sqrt{S_{d_2}^2(\omega_0 + \omega) + S_{d_2}^2(\omega_0 - \omega)} \quad [\text{deg/hr/rt-Hz}] \quad (6)$$

where it is understood that the frequency variable ω is constrained from DC to the bandwidth of the low-pass filter. A further simplification can be made using the fact that ω_0 is at least an order of magnitude larger than the low-pass filter bandwidth,

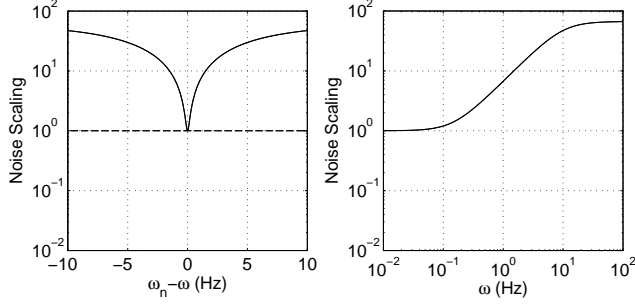
$$\begin{aligned} S_{\Omega}(\omega) &\approx \frac{4\sigma m \mu}{K_{s_2}\alpha a\omega_0} \sqrt{\frac{\Delta^2 + \sigma_{clp}^2}{\sigma^2}} \\ &\times \sqrt{\frac{\left(\Delta^2 + \omega^2 + \sigma_{clp}^2\right) \left(\Delta^2 + \omega^2 + \sigma_{eff}^2\right) - (2\Delta\omega)^2}{\left[(\Delta - \omega)^2 + \sigma_{clp}^2\right] \left[(\Delta + \omega)^2 + \sigma_{clp}^2\right]}} \end{aligned} \quad (7)$$

where the *effective bandwidth*, denoted σ_{eff} , is defined as

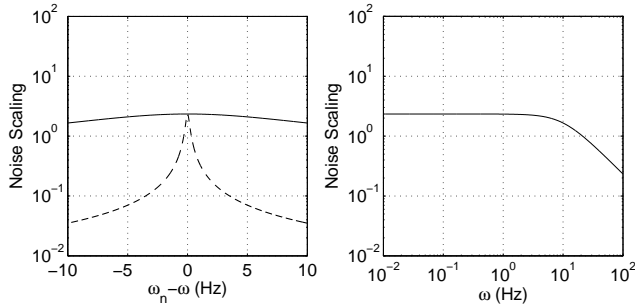
$$\sigma_{eff} = \sigma \sqrt{1 + h^2 \frac{v^2}{\mu^2}}. \quad (8)$$

In the case when $\omega_0 = \omega_n$, i.e. the demodulation frequency coincides with the notch in (4), the spectral density of the closed-loop rate-equivalent noise reduces to

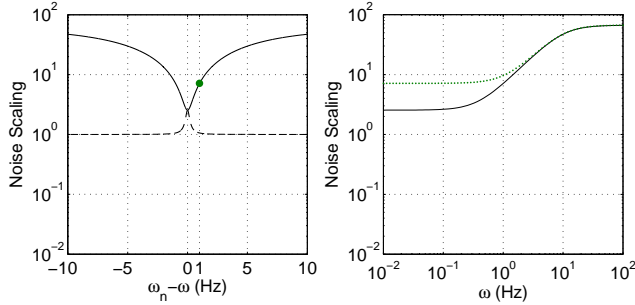
$$S_{\Omega}(\omega) = \frac{4\sigma m \mu}{K_{s_2}\alpha a\omega_n} \cdot \frac{\sigma_{clp}}{\sigma} \sqrt{\frac{\omega^2 + \sigma_{eff}^2}{\omega^2 + \sigma_{clp}^2}} \quad (9)$$



(a) $v = 0, \mu \neq 0, \Delta = 0\text{Hz}$



(b) $v \neq 0, \mu = 0, \Delta = 0\text{Hz}$



(c) $v \neq 0, \mu \neq 0, \Delta = 0\text{Hz}$ (black, solid), $\Delta = 1\text{Hz}$ (green, dotted)

Fig. 2. (Left) Noise scaling for open-loop (dashed) and closed-loop rate-equivalent noise (solid) prior to demodulation. (Right) Noise scaling for post-demodulated closed-loop rate-equivalent noise with $\sigma_{clp} = 10\text{Hz}$. The model's mechanical bandwidth is 0.15Hz with $\omega_n = 15\text{kHz}$ and $Q = 50\text{K}$.

This spectral density possesses a high-pass filter characteristic as long as the closed-loop bandwidth is larger than the effective bandwidth, i.e., $\sigma_{clp} > \sigma_{eff}$. The low frequency asymptote, (9) evaluated at $\omega = 0$, matches the lowest rate-equivalent noise density of the signal prior to demodulation (5). The flat, low-frequency noise density, indeed, corresponds to the angle random walk (ARW) of the angle estimate [4], which is invariant with respect to the closed-loop bandwidth. When the noise is dominated by electrical noise, e.g., $\mu \neq 0$ and $v = 0$, the ARW is inversely proportional to the modal quality factor Q , whereas the ARW only reduces in proportion to \sqrt{Q} if mechanical-thermal noise dominates, e.g., $\mu = 0$ and $v \neq 0$. Detuning has

a detrimental effect on the rate-equivalent noise by raising the low frequency noise floor thereby degrading the sensor's ARW figure. When $\Delta < \sigma_{clp}$, i.e. the degree of detuning is less than the closed-loop bandwidth, the ARW is given by

$$\frac{4\sigma m}{K_{s_2} \alpha a \omega_n} \sqrt{\left(\frac{\Delta^2}{\sigma^2} + 1\right) \left(\mu^2 + \frac{\sigma^2}{\sigma^2 + \Delta^2} h^2 v^2\right)}, \quad (10)$$

which is always larger than (5). Fig. 2 illustrates the individual and combined contributions of electrical and mechanical-thermal noise to the rate-equivalent noise prior to demodulation as well as post-demodulation by plotting the noise scaling for different cases. The noise scaling is defined as the noise density normalized by the reference case that is corresponding to the tuned open-loop case with $v = 0$ (noise density of s_2 in the absence of feedback signal, $d_2 = 0$). The reference case is one for all frequencies and plotted as a dashed line in 2(a). When both electrical and mechanical-thermal noise are present in 2(c), the open-loop noise scaling prior to demodulation shows a flat spectrum with a peak at the resonant frequency and the deep notch of the closed-loop noise at the resonant frequency coincides with the peak as expected. The low frequency floor of the post-demodulated closed-loop noise scaling also matches the peak. For a 1Hz detuned case in 2(c), the raised low frequency floor of the post-demodulated closed-loop noise scaling well matches the dot marked 1Hz away from the resonant frequency on the closed-loop noise scaling prior to demodulation.

III. EXPERIMENTAL RESULTS

Boeing's Disk Resonator Gyro (DRG) is a high-performance MEMS vibratory gyro whose vibrating structure has an 8mm diameter disc-shaped resonator that is composed of a number of thin concentric rings connected by spokes. The central post of the resonator is rigidly attached to the baseplate so that the rings are free to vibrate in the plane of the resonator and electrodes fixed to the baseplate are embedded in the gaps between the rings for electrical actuating, sensing, and biasing. A buffered input voltage applied to an actuating or driving electrode generates a radial electrostatic force to excite the resonator and a sensing electrode employing a transresistance amplifier converts the subsequent in-plane vibration into a buffered output voltage that is proportional to a radial velocity of the ring. The sensing and driving electrodes are configured in pairs so as to exploit the resonator's fundamental Coriolis-coupled modes. More details on the DRG may be found in [8].

The ideal sensor is designed to operate in a degenerate condition in which two Coriolis-coupled modes have equal resonant frequencies, however, a modal frequency split in the "native" resonator is unavoidable due to manufacturing imperfections and process variations. For example, Fig. 3 shows empirical frequency response magnitudes of the two-input/two-output open-loop sensor dynamics in a neighborhood of the Coriolis-coupled modes for both the native sensor dynamics and the "tuned" sensor dynamics. The biasing electrodes are crucial in tuning the sensor dynamics by providing constant potentials between the resonator and

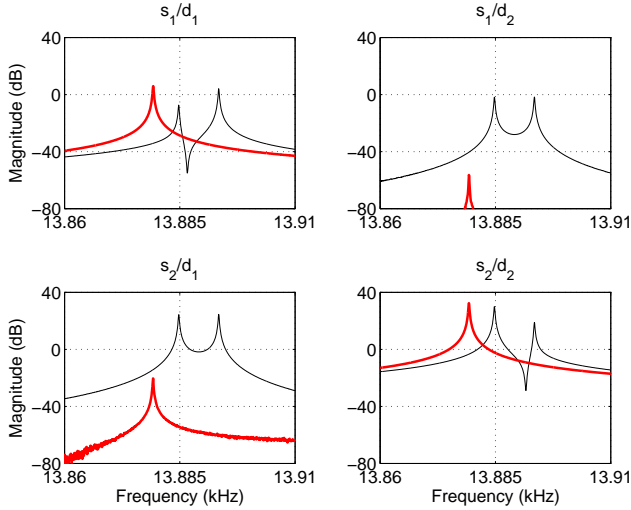


Fig. 3. Empirical frequency response of the DRG. Two-input/two-output magnitude plots of the DRG in its “untuned” native state (black, thin) when all the tuning bias potentials are equal to the resonator bias suggest that the modal frequency split is 8.6Hz. The peak gains of diagonal channels are different since the output signal conditioning dynamics’ gains are optimized for each loop. When the sensor is electrostatically tuned (red, thick), only a single peak is evident in each channel and cross-channel couplings are significantly reduced. Note that the inputs (d_1, d_2) and outputs (s_1, s_2) are in volts and only the magnitudes are plotted to keep the figures uncluttered.

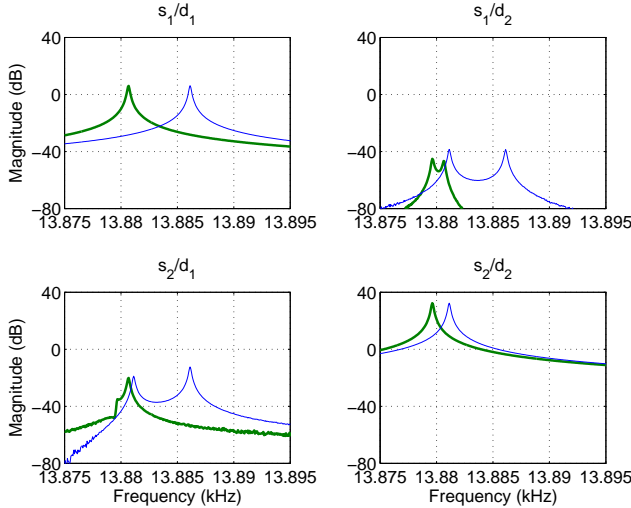


Fig. 4. Empirical frequency response of the DRG when the sensor dynamics are detuned by 1Hz (green, thick) and 5Hz (blue, thin) to demonstrate the effect of detuning on the rate-equivalent noise. The modes are still decoupled even though they are detuned.

the electrodes which electrostatically modifying the sensor’s stiffness to yield degenerate modal frequencies. The electrostatic tuning algorithm based on parametric model estimation reported in [5] is quite effective in tuning and decoupling the sensor dynamics or even detuning the sensor dynamics to a targeted split while maintaining decoupling. The empirical frequency response magnitudes of the tuned sensor in Fig. 3 exhibit lower modal frequencies than the native modal fre-

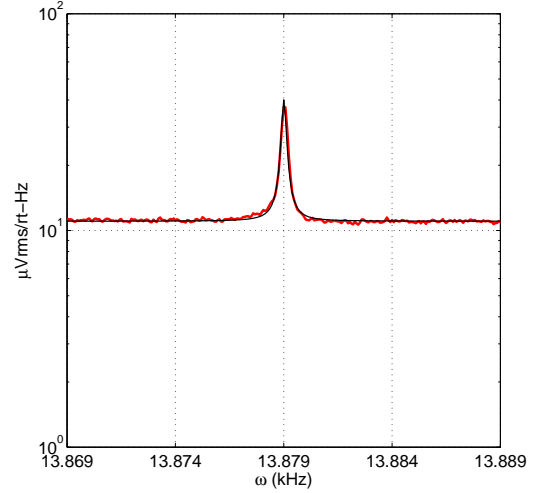


Fig. 5. Measured open-loop voltage spectrum of the sense channel noise (red) and the model fit to the data (black). The flat portion of the spectrum is caused by thermal noise in the buffer amplifier resistor and yields $\mu = 11 \times 10^{-6} \text{V}_{\text{rms}}/\text{rt-Hz}$. The sharp spike is mechanical-thermal noise in the resonator and yields $v = 0.93 \times 10^{-6} \text{V}_{\text{rms}}/\text{rt-Hz}$. Computing v requires the frequency response data in Fig. 3

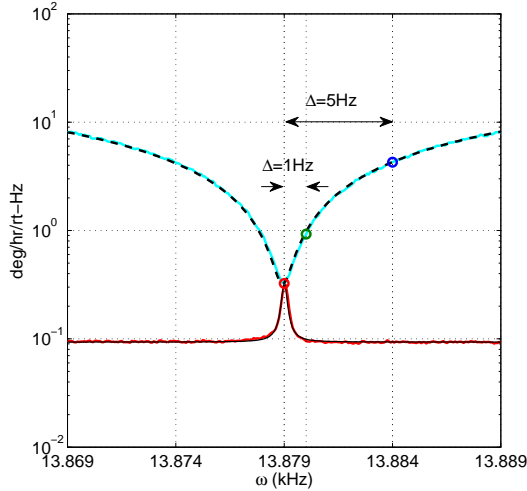
quencies because electrostatic biasing introduces a softening spring effect. Fig. 4 shows two cases of detuned sensor dynamics with target splits of $\Delta = 1 \text{Hz}$ and $\Delta = 5 \text{Hz}$. These cases will be used to demonstrate the effect of detuning on the angular rate noise spectrum.

The decoupled sensor dynamics, whether tuned or detuned, means the off-diagonal channels can be ignored in the noise analysis and feedback compensators can be independently synthesized for each diagonal channel. For the DRG, a nonlinear automatic gain control (AGC) is implemented for the excitation loop to maintain a stable harmonic oscillation of the s_1 signal. The oscillation frequency, which is the demodulation frequency, is equal to the modal frequency in the “ s_1/d_1 ” channel in Fig. 3. This frequency was denoted ω_0 in the previous analysis. A high gain feedback filter is used for the rebalance channel to regulate s_2 . The modal frequency of the “ s_2/d_2 ” channel in Fig. 3 was denoted ω_n in the previous analysis. The reader is referred to [1] for a detailed analysis on the controller design. A PC-based DSP board is used for the real-time filter implementation as well as the signal processing for the angular rate estimation. These details are secondary to the objectives of this paper and are not presented.

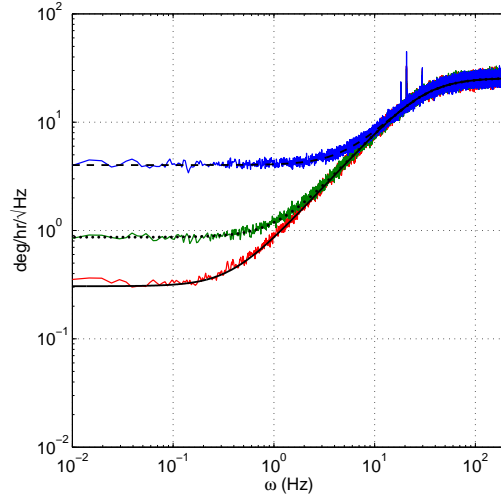
The noise analysis requires the open-loop spectral density of the sense channel noise (shown in Fig. 5) and the transfer function of the sense channel. The noise spectrum yields

$$\begin{aligned} \mu &= 11 \times 10^{-6} \text{V}_{\text{rms}}/\text{rt-Hz}, \\ v &= 0.93 \times 10^{-6} \text{V}_{\text{rms}}/\text{rt-Hz} \\ \omega_n &= 13879\text{Hz} \\ \sigma &= 0.10\text{Hz} \end{aligned}$$

The transfer function is obtained by fitting a model to the



(a) Rate-equivalent noise density prior to demodulation



(b) Rate-equivalent noise density of the estimated rate

Fig. 6. (Left) Rate-equivalent noise densities of open-loop (red) and closed-loop (cyan) sense channel prior to demodulation. Model predictions are plotted with solid and dashed traces for open-loop and closed-loop cases, respectively. (Right) The closed-loop rate-equivalent noise densities of the estimated angular rate when the sensor is tuned (red), detuned by 1Hz (green), and detuned by 5Hz (blue). For each case, the low frequency noise floor is very close to the value marked by its corresponding circle in (a). Model predictions are plotted with solid, dotted, and dashed traces for tuned, 1Hz detuned, and 5Hz detuned cases, respectively.

“ S_2/d_2 ” data associated with the tuned case in Fig. 3. This model is given by

$$H_g(s) = \frac{54.1s}{s^2 + 2(2\pi \times 0.1035)s + (2\pi \times 13879)^2} \quad (11)$$

Scaling the open-loop voltage spectrum by the demodulation amplitude and DRG scale factor (both are empirically determined) yields the open-loop rate-equivalent spectral density as well as the closed-loop rate-equivalent spectral density that is given by (4). For the closed-loop case, $K_{reb} = 7$ yields $\sigma_{clp} = 30\text{Hz}$. These spectra are shown in Fig. 6(a). Small perturbations to ω_0 do not change these spectra, while small perturbations to ω_n only shift the frequency where the spike/notch occurs. Fig. 6(b) shows the corresponding closed-loop rate-equivalent noise densities of the angular rate estimate (post-demodulation) for the cases when $\Delta = \{0, 1, 5\}\text{Hz}$ (from Figs. 3 and 4). The important parameter is Δ , which determines the demodulation frequency relative to the notch in Fig. 6(a). When $\Delta = 0$ the demodulation frequency coincides with the deepest part of the notch in Fig. 6(a) –this imparts the lowest possible noise floor in the angular rate spectrum at low frequencies. If the sensor modes are detuned, however, the demodulation frequency moves to a part of the spectrum in Fig. 6(a) where the spectral density has a higher value thereby producing a higher noise floor in the angular rate spectrum. These trends are evident in Fig. 6(b). Note that these figures also show the prediction of the model based on the values of μ , ν , H_g , K_{reb} and Δ . The model agreement with the data is extremely good.

IV. CONCLUSIONS

We have presented a comprehensive spectral density model of the closed-loop rate-equivalent noise for vibratory rate

gyro whose dominant noise sources are pick-off noise and mechanical-thermal noise in the sense channel. The spectral density approach is very useful in explaining the effects of sensor parameters on the angular rate noise spectrum. This paper focused on modal detuning, however, perturbations to the resonator quality factor and closed-loop bandwidth can also be explored with this noise model. Details of the impact of the sigmoid-shaped angular rate noise spectrum on the integrated angular rate noise spectrum, especially with regard to the sensor’s angle random walk figure, will be reported in future papers.

REFERENCES

- [1] Chen, Y.-C., M’Closkey, R.T., Tran, T.A., and Blaes, B., “A control and signal processing integrated circuit for the JPL-Boeing micromachined gyroscopes,” *IEEE Trans. Control System Technology*, Vol. 13, No. 2, 2005, pp. 286-300.
- [2] Gabrielson, T. B., “Mechanical-thermal noise in micromachined acoustic and vibration sensors,” *IEEE Trans. Electron Devices*, vol. 40, no. 5, May 1993, pp. 903-909.
- [3] Johnson, J. B., “Thermal agitation of electricity in conductors,” *Physical Review*, vol. 32, July 1928, pp. 97-109.
- [4] Kim, D., and M’Closkey, R. T., “Dissecting tuned MEMS vibratory gyros,” book chapter in *Feedback Control of MEMS to Atoms*. Gorman, Jason J.; Shapiro, Benjamin (ed.), October 2011, Springer.
- [5] Kim, D.-J., and M’Closkey, R.T., “A systematic method for tuning the dynamics of electrostatically actuated vibratory gyros,” *IEEE Trans. Control System Technology*, Vol. 14, No. 1, 2006, pp. 69-81.
- [6] Leland, R. P., “Mechanical-thermal noise in MEMS gyroscopes,” *IEEE Sensors Journal*, Vol. 5, No. 3, 2005, pp. 493-500.
- [7] Papoulis, A., *Probability, Random Variables, and Stochastic Processes*, Third Ed., 1991, McGraw-Hill.
- [8] To, A.C., Liu, W.K., Olson, G.B. et al., “Materials integrity in microsystems: a framework for a petascale predictive-science-based multiscale modeling and simulation system,” *Comput. Mech.*, vol. 42, 2008, pp 485-510.